Analysis of power losses in an industrial planetary speed reducer: Measurements and computational fluid dynamics calculations

Franco Concli, Edoardo Conrado and Carlo Gorla

Date received: 15 March 2013; accepted: 17 June 2013

Introduction

Advantages of planetary speed reducers are well known and due to their compact design and high power density they are suitable for a wide range of applications. Although planetary gear transmissions show in general very high efficiency levels, the increasing demand for reduction of energy consumption in all technical applications calls for a further reduction of power losses also in this type of gearboxes. Moreover, reduced power losses within the gearbox favorably impact its thermal load-carrying capacity which can also be a critical characteristic in this type of transmissions due to their high power density.

Sources of power losses in a gearbox can be classified into two groups: load-dependent and load-independent power losses. The load-dependent power losses of a gearbox are functions of the transmitted power and become zero when the transmitted torque sinks to zero. They are mainly due to friction losses at the loaded gear and bearing contacts and thus depend on the acting force between the solids, the sliding speed and the coefficient of friction present at the contact between the surfaces. The load-dependent power losses have already been deeply investigated and reliable models are available for estimating them.[1] The load-independent power losses are not affected from the transmitted load and exist also if the transmitted torque is zero. No-load losses comprise all losses which exist when the gearbox is not transmitting power, but only rotating without output torque. Losses in seals belong to no-load losses. Other no-load losses derive from the interaction of the moving/rotating elements of the transmission and the air/lubricant mixture.

Carrying out a deeper analysis, the no-load losses of the gears can be subdivided into churning, windage and oil squeezing power losses. The churning power losses are related to the viscous and pressure effects of the air/oil lubricant mixture on the

Dipartimento di Meccanica, Politecnico di Milano, Milano, Italy

Corresponding author:
Edoardo Conrado, Dipartimento di Meccanica, Politecnico di Milano, via La Masa 1, 20156 Milano, Italy.
Email: edoardo.conrado@polimi.it

moving/rotating elements. The amount of this kind of losses is strongly dependent from the lubricant quantity and properties and from the gearbox configurations, but, generally speaking, they represent the largest share of the no-load losses of the gears. The windage power losses are similar to the churning ones, but involve only one phase (air or oil) and not a multiphase lubricant mixture. This kind of losses becomes significant especially for gears where the tangential speed becomes important like gears with high rotational speeds.[2,3] The last fraction of the no-load losses of the gears, the oil squeezing one, is related to the changing volume of the gap at the mesh position during the engagement causing an overpressure that squeezes the oil out causing additional power losses.

For the specific case of planetary gears, the load-independent power losses are given by four contributions: churning power losses due to the rotation of the gears about their axes, churning power losses due to the motion with a circular path of the planets due to the rotation of the planet carrier on which they are mounted, no-load losses of bearings and seal losses.

While a large amount of work dealing with load-dependent gear power losses is available (see e.g. ref.[4] for the specific case of planetary gears), the literature on load-independent losses in dip lubricated gears is limited. A pioneering study in this field was performed by Ohlendorf[5] that experimentally obtained a formulation for the estimation of the churning power losses for a splash lubricated single gear and one of the most complete works is that proposed by Mauz,[6] who has concentrated on hydraulic losses of cylindrical gears. Subsequent studies by Terekhov[7] analyzed the influence of rotational speed, module, immersion depth, gear diameter, tooth face width, gear ratio and oil viscosity on the churning and squeezing power losses for splash lubricated gears. The formulation proposed by Terekhov was subsequently extended by Walter and Langenbeck [8] and Walter.[9] More recent studies about the churning power losses were performed by Changenet and Velex.[10] The results proposed by them are based on dimensional analysis and have been experimentally validated over a wide range of speeds, gear geometries, lubricants and immersion depths.

In this paper, results of efficiency tests conducted on an industrial planetary speed reducer in various operating conditions showing the contributions of load-dependent and load-independent power losses to the total power loss are presented. A numerical methodology, based on computational fluid dynamics (CFD) analysis, in which the authors can prove previous effective applications to ordinary gears,[11] able to evaluate gear load-independent power losses in planetary speed reducers taking into account the real gearbox configuration and operating conditions is proposed. Finally, the different contributions to the total efficiency were also calculated by means of analytical models available in the literature and CFD analyses, summed together and compared with the total efficiency measurements in order to show the effectiveness of the adopted calculation models.

Experimental tests

The gearbox under investigation is an industrial planetary speed reducer, produced by the Tecnoingraggi division of the Bonfiglioli Group and commercially available under the trade name MP IS 105-1-4. The MP IS 105 is a small size planetary speed reducer of the series MP that is mainly employed in industrial automation applications. The main geometric and load-carrying capacity characteristics are listed in Table 1 and the longitudinal section of this speed reducer is shown in Figure 1. The MP IS 105-1-4 is a single-stage planetary speed reducer with a 1:4 ratio in which the power enters from the sun gear shaft and, after being transmitted through three planet gears, exits from the planet carrier output shaft, being the annulus gear fixed. The input and the output shafts are both supported by a pair of ball bearings and needle rollers are interposed between the three planet gears and their pins. The main geometrical and load-carrying capacity characteristics of these rolling bearings are listed in Table 2. The housing is sealed by means of radial shaft-ring seals with a single lip mounted on both the input and the output shafts. The planetary gear train is dip lubricated with 58 g of a synthetic gear lubricant on a polyglycol basis (Klüebersynth GH 6-220) corresponding to a static oil level at 25°C that reaches the rolling elements of the ball bearings mounted on the input shaft. The main physical properties and characteristics of this lubricant are listed in Table 3.

Test apparatus

Efficiency tests were performed on an electrically closed-loop DC motor/brake test bench in order to measure the total power losses of the speed reducer as well as the contributions of the load-dependent and

Table 1. Main characteristics of the planetary gearbox.

Parameter	Unit	Value
Nominal output torque	(Nm)	140
Maximum output torque	(Nm)	210
Nominal input rotational speed	(r/min)	2800
Maximum input rotational speed	(r/min)	4500
Maximum operating temperature	(°C)	90
Number of stages	(–)	1
Number of planets	(–)	3
Number of teeth sun gear	(–)	36
Number of teeth ring gear	(–)	108
Number of teeth planet gears	(–)	36

load-independent power losses. An image and a scheme of the test bench are shown in Figure 2. The test rig was constituted by a 30 kW brushed DC electric motor and a 30 kW dynamo acting as a brake. Each of them was equipped, at the output and the input respectively, with in-line LEBOW strain gauges torque meters with slip rings transmission systems integrated by speed sensors, which measured the torque and the speed at the output of the motor and at the input of the brake.

These two torque sensors (Lebow model 1104 2 k) had a nominal rated torque of 225 Nm and their main metrological characteristics are listed in Table 4. The speed reducer, which was supported by a structure fixed to ground and rigidly connected to its case, was connected to the motor and brake by means of double Cardan joint drive shafts in order to compensate small misalignments. Two supporting systems with bearings are present between each torque meter and the corresponding double Cardan shaft. An additional in-line torque transducer, an HBM T12 torque flange with a telemetric transmission system was directly connected to the input shaft of the reducer. The HBM T12 digital torque transducer had a nominal rated torque of 500 Nm and its metrological characteristics are listed in Table 4. The test rig was controlled by means of a closed-loop control system so that during the tests the input speed and the output (braking) torque could be imposed. The test rig was equipped also with two thermocouples applied on the speed reducer case and another one on the case of the support located between the speed reducer and the torque meter. These temperature sensors were three type T thermocouples with a tolerance of $\pm 1.0^{\circ}$C and a temperature range from 0°C to 370°C.

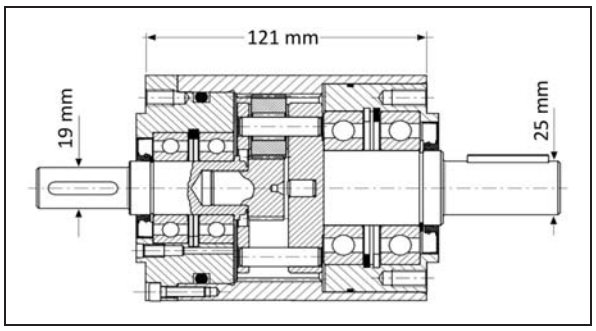

Figure 1. Longitudinal section of MP105-1-4 IS planetary speed reducer.

Test performed

The planetary speed reducer was tested at three different rotational speeds of the input shaft, 1500, 2000 and 2800 r/min with an imposed braking torque of 120Nm in order to measure the global efficiency and power losses in the speed reducer at these operating conditions. During the tests, the temperature of the speed reducer was monitored by the two thermocouples mounted on the gearbox case and the temperature of the support was measured by the third thermocouple, as well. All the tests started at room temperature of 23°C in an air conditioned laboratory and ended when a thermal steady-state regime was reached, i.e. when the measured temperature of the housing was constant. All the load, speed and temperature data were acquired synchronously from all the measurement devices for 5 s after a variation of 5°C of the temperature of the housing or after 10 min.

In order to evaluate the no-load power losses at the thermal steady-state conditions reached for the three different rotational speeds of the input shaft, additional tests were conducted at zero output torque immediately after the end of each test at 120Nm.

Measured quantities

The aim of the tests performed was the determination of global efficiency and power losses in the

Table 3. Main physical properties and characteristics of the lubricant.

Klübersynth GH6 220		
Property	Unit	Value
Base oil type	(–)	Polyglycol oil
ISO VG (DIN 51519)	(–)	220
Density at 15°C (DIN 51757)	(kg/m^3)	1060
Kinematic viscosity at 20°C	(mm^2/s)	630
Kinematic viscosity at 40°C	(mm^2/s)	220
Kinematic viscosity at 100°C	(mm^2/s)	40
Viscosity index (DIN ISO 2909)	(–)	$>=220$

Table 2. Main geometrical and load-carrying capacity characteristics of the rolling bearings.

	Inner diameter	Width	Outer diameter	Dynamic load coefficient	Max speed
Symbol Unit	d (mm)	B (mm)	D (mm)	C (kN)	n_{lim} (r/min)
Input shaft bearings (SKF 6205)	25	15	52	14.8	18,000
Output shaft bearings (SKF 6207)	35	17	72	27	13,000
Planet needle rollers and cage assembly	9	15	13	–	–

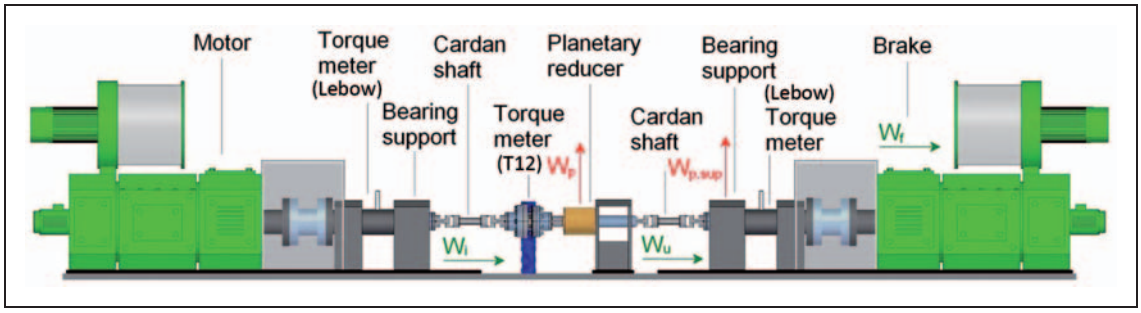

Figure 2. A schematic layout of the test rig with the planetary speed reducer under test.

Table 4. Metrological characteristics of the torque transducers.

Torque transducer	HBM T12	Lebow 1104 2 k
Full range (Nm)	500	225
Sensitivity tolerance (% of max torque)	0.01[a]	0.05
Linearity deviation incl. Hysteresis (% of full range)	0.01	0.1
Temp deviation on the zero point per 10 K deviation from 23°C (% of full range)	0.02	0.002
Temp deviation on the sensitivity per 10 K deviation from 23°C (% of max torque)	0.03	0.002
Standard deviation of the repeatability (of max torque)	0.01	0.05

[a]According to the calibration certificate.

speed reducer. The total power loss in the speed reducer was indirectly determined as the difference of the input and the output power, that is:

$$W_p = W_i - W_u$$

The speed and torque measured by the HBM T12 torque transducer, directly connected to the input shaft of the gearbox, gave directly the input power W_i of the speed reducer. On the contrary, the power W_f measured before the brake by the Lebow torque transducer was lower than the actual output power W_u of the reducer, due to the power losses of the components $W_{p,sup}$ interposed between the speed reducer output shaft and the torque meter. Therefore, the output power of the speed reducer was determined as follows:

$$W_u = W_f + W_{p,sup}$$

In order to determine the values of $W_{p,sup}$ as a function of the temperature of the supporting systems, preliminary tests without the speed reducer have been performed and the losses have been measured at different temperatures. In this way their values, at the corresponding test temperature of the support, can be introduced in the previous equation and the output power of the speed reducer can be calculated. The power losses in the double Cardan joint drive shaft were assumed to be negligible since this shaft worked quasi-perfectly aligned during the tests.

The total power loss W_p in the speed reducer is the sum of power losses dependent and independent from the transmitted load. The load-independent losses $W_{p,indep}$ were directly measured in the additional tests at zero output torque previously mentioned and, therefore, also the load-dependent losses $W_{p,dep}$ can be calculated as

$$W_{p,dep} = W_p - W_{p,indep}$$

Finally, the global efficiency of the planetary speed reducer can be indirectly measured from these quantities as the ratio of the output power to the measured input power, that is

$$\eta = \frac{W_u}{W_i} = \frac{W_f + W_{p,sup}}{W_i}$$

Model of power losses

The global efficiency of the gearbox depends on the contribution of all the source of losses. In the analyzed planetary speed reducer, the total losses are given by the sum of the load-dependent and load-independent losses of the bearings and gears and the losses of the seals. According to ref.,[1] the total power losses of geared transmissions can be subdivided as follows:

$$P_V = P_{VZ0} + P_{VZ} + P_{VB0} + P_{VB} + P_{VD} + P_{VX}$$

that is, the sum of the losses generated by the gears (subscript Z), by the bearings (subscript B), by the contact seals (subscript D) and other miscellaneous

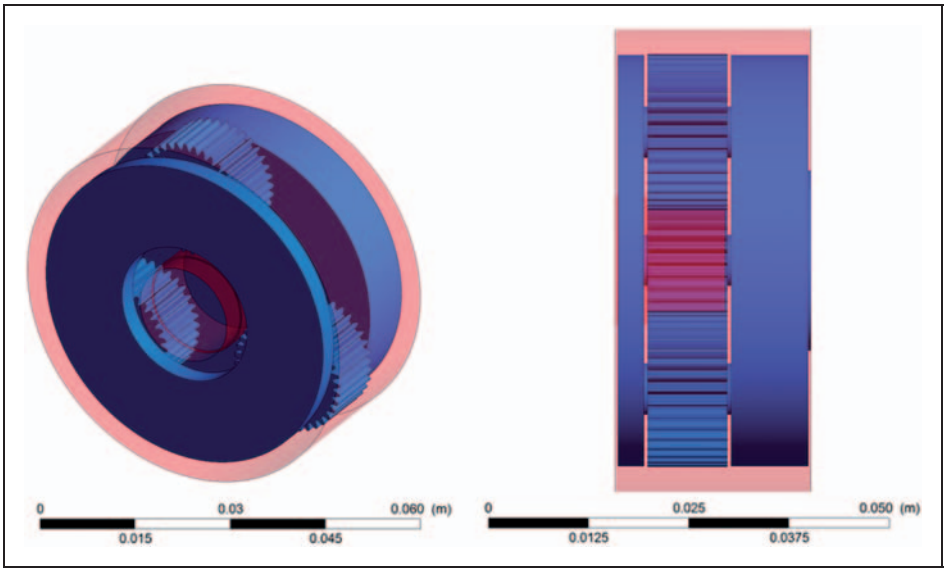

Figure 3. Boundaries of the computational domain used for the CFD analyses about the churning losses of the planet carrier. 'Rotating boundaries' corresponding to the planet carrier together with the planets and 'static boundaries' corresponding to the internal walls of the case of the speed reduces and the external surfaces of the sun gear: isometric view on the left and lateral view on the right.
CFD: computational fluid dynamics.

losses (like clutches and synchronizers) (subscript X). The total losses can be furthermore subdivided into load-dependent and load-independent ones (subscript 0).

The losses of the bearings have been deeply investigated in the past decades and accurate models are available. Therefore, these losses have been calculated according to one of these models.[12] The seal losses have been calculated according to ref.[1] Also for the load-dependent power losses of gears the literature provides some adequate models. In particular, the models proposed by the ISO/TR 14179 technical report[13,14] have been applied.

Concerning gears, carrying out a deeper analysis, the no-load losses of the gears P_{VZ0} can be furthermore subdivided into churning $P_{VZ0,C}$, windage $P_{VZ0,W}$ and oil squeezing $P_{VZ0,S}$ power losses.

$$P_{VZ0} = P_{VZ0,C} + P_{VZ0,W} + P_{VZ0,S}$$

The amount of these load-independent power losses is strongly dependent on the gearbox configuration and the operating conditions becoming, in general, important in planetary speed reducers. Besides the common churning losses due to the rotation of the gears and the squeezing losses due to the gear meshing, in the planetary speed reducers, the presence of the planet carrier induces additional losses. This rotating structure, in fact, interacts with the lubricant generating additional churning losses.

For the calculation of all this load-independent losses, a novel approach based on CFD has been used. This technique is based on the solution of five transport equations for mass, momentum (three equations) and energy.

The solving procedure is based on the discretization of the domain and the application of the transport equations to each small partition. In this manner it is possible to obtain the pressure and velocity fields in the whole domain and from these the resistant torque and, consequently, the power losses can be calculated.

Churning power losses due to planet carrier

The first and most important contribution to the load-independent power losses in a planetary speed reducer is related to the presence of the planet carrier. Due to its rotation, the planets that are mounted on it have a motion in a circular path around the gearbox axis, which induces additional losses.

In order to estimate them, a CFD model has been applied.[15] The model reconstructs the whole internal volume of the speed reducer, but neglects the teeth of the sun gear and of the external crown. In this manner the planets result unengaged and do not rotate around their axis. So it is possible to calculate the losses related only to the presence of the planet carrier. Figure 3 shows the computational domain. In the tested speed reducer, the boundaries corresponding to the planet carrier together with the planets (highlighted in blue/dark gray in Figure 3) rotate around the gearbox axis and are therefore called 'rotating' or 'dynamic boundaries'. The remaining boundaries (highlighted in red/light gray in Figure 3) corresponding to the internal walls of the case of the speed reduce and the external surfaces of the sun gear are steady and do not rotate during the simulations.

In order to be able to perform a CFD simulation that correctly reproduces this configuration, some

particular techniques should be used. In particular a 'dynamic mesh' should be created. In a classical CFD approach, the motion of the boundaries corresponding to the planet carrier plus the planets (blue/dark gray boundaries in Figure 3) distorts the mesh that should be updated and corrected after few iterations. In order to circumvent this, a rigid motion has been applied to the whole mesh. In this manner the motion of the planet carrier plus the planets is guaranteed and the stationarity of the internal walls of the case of the gearbox is than reconstructed applying opposite velocities on the static boundaries. The rigid rotation of the whole mesh, in fact, implies also a rigid rotation to the 'stationary boundaries' (red/light gray ones) as collateral effect. By applying an opposite velocity boundary condition it is possible to compensate this and to reproduce the right condition in which the velocity of the fluid on the steady boundaries is zero. In this manner, the right boundary conditions are reproduced avoiding mesh deformation and the consequent mesh handling problems.

As an example of the results obtainable, Figure 4 shows the contour plots of the lubricant volume fraction for two different oil levels. It can be seen that the lubricant lies primarily on the modified annulus thanks to the centrifugal force. In the simulations the lubricant level was set equal to the measured static oil level at 25°C before running the code at the operating temperature (the energy equation was not activated so the temperature was set by manually changing the oil properties before any simulations). The volume variation of the oil in a first approximation has been considered negligible.

The resistant torque was calculated with a surface integral on the moving walls with respect to the gearbox axis and was composed of two parts: the first given by pressure and the second by the viscous effects. The product of this resistant torque by the rotational speed of the planet carrier is directly the power loss.

Churning power losses due to the rotation of gears

Another contribution to churning power losses is due to the rotation of gears about their axes. This second source of churning losses has also been studied by a CFD-based approach. As before, the churning losses due to the gear rotation arise from the interaction with the oil/air lubricant mixture and are strongly affected by the operating and geometrical parameters. In this case, for each gear, a stand-alone model has been made ready. In order to be able to model the rotation of the gear, a specific concept has been adopted: sliding mesh. This technique allows applying the rotation to the gear boundaries avoiding mesh deformation. In other words, the gear geometry is immersed in a cylindrical domain. This first rotating domain is surrounded by another domain in which a cylindrical cavity is present. In this manner the motion of the internal domain ensures the rotation of the gear boundaries avoiding mesh deformation. At this point the two domains result numerically uncoupled, so an interface should be defined. The parameter adopted for the simulations is shown in Table 5.

Unlike the simulations of the churning losses due to the planet carrier, in this case the higher rotational speeds necessitated a turbulence model. The averaged Navier–Stokes equations have, in comparison with the not-averaged equations, an additional term τ_{ij} called unresolved term. The averaging process produces a set of equations that is not closed. For this reason a turbulence model is needed in order to be able to solve the system of equations.

The unresolved or Reynolds terms are expressed by using the eddy-viscosity hypothesis. The re-normalization group model assumes that the eddy

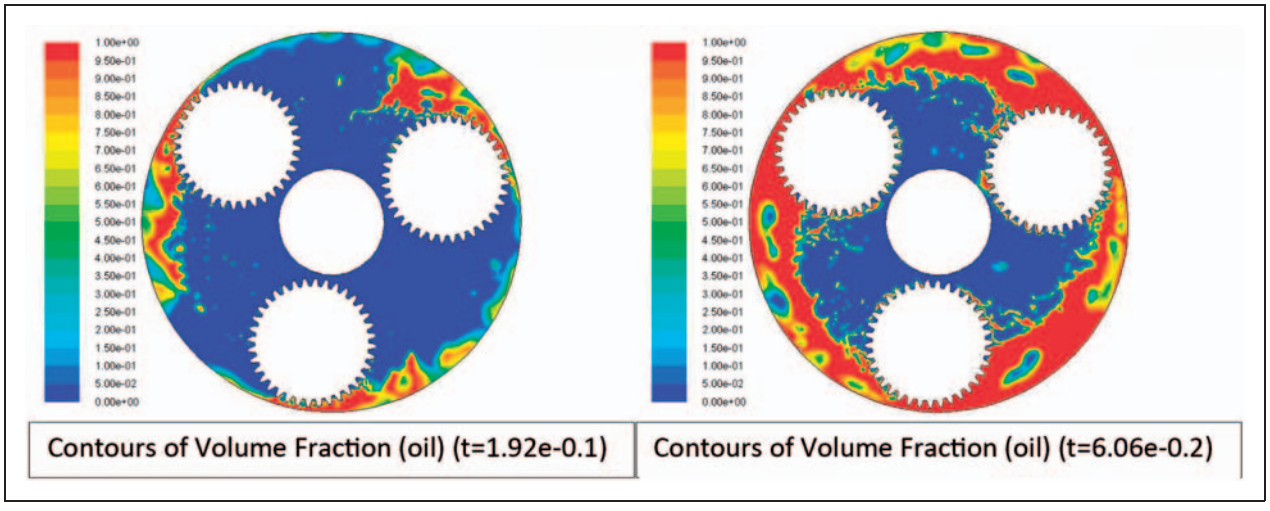

Figure 4. Contour plots of the lubricant volume fraction for two different oil levels in the steady condition in the symmetry plane of the planets.

viscosity is related to the turbulence kinetic energy and dissipation via the relation

$$\mu_t = C_\mu \rho \frac{k^2}{\varepsilon}$$

The model transport equation for k is derived from the exact equation, while the model transport equation for ε was obtained using physical reasoning and bears little resemblance to its mathematically exact counterpart.[16] Some other more complex turbulent models exist, but some researchers claim that this model offers improved accuracy in rotating flows.[17] For this reason this turbulence model was selected to perform the simulations.

Squeezing power losses

In the engaging zone of a gear pair, the volume of the cavity between the teeth is continuously changing due to the gear mating. The sudden reduction in the volume filled with lubricant causes an overpressure and, consequently, a fluid flow primarily in the axial direction. After reaching the minimum value, the volume increases again and a consequent fluid flow takes place from the oil bath to the cavity between the teeth. This process is cyclic and, in general, there are multiple cavities that are squeezed together. Due to the viscous properties of the lubricant, this phenomenon induces power losses.

This phenomenon has been deeply investigated by the authors in a previous paper.[18] For the estimation of this kind of losses a simplified domain consisting of the only mating zone has been modeled. The simulation parameters are the same as Table 5 except for the volume of fluid (VoF) model that was not necessary.

In order to be able to perform this kind of simulations, it is important to be able to properly manage the mesh during the calculations. The motion of the boundaries, in fact, causes a stretch of the mesh. If the mesh is not updated in order to absolve prescribed skewness criteria, it will collapse after some time steps. For these simulations a spring-based smoothing method coupled with local remeshing has been used (see Figure 5).

In other words, due to the motion of the boundaries, the computational domain is topologically changed after each time step and the mesh is therefore deformed. In the spring-based smoothing method, each element of the mesh is treated as a spring. The initial spacing between the elements represents the equilibrium state of the virtual net of springs. When a node (that belongs to the boundary) moves due to a prescribed boundary motion, the whole mesh is adjusted in order to find a new equilibrium state. In this manner, it is possible to also apply big boundary motions avoiding cell collapse. The remeshing technique is used when the smoothing is not enough. Some extra distorted element are locally deleted and substituted with new ones.

Results and discussion

The results of experimental tests performed at three different rotational speeds of the input shaft are shown in Figure 6 in terms of global efficiency versus test time, while in Figure 7 the variation of the temperatures measured during the tests by the two thermocouples placed on the housing of the speed reducer is shown. The temperature of the housing reached at the thermal steady-state condition increased with the rotational speed, as might be expected due to the different amount of mechanical input power in the three operating conditions. Also the time required to reach the steady-state condition obviously increased. On the contrary, the steady-state efficiency of the planetary gearbox showed to be only slightly influenced by the rotational speed.

Table 5. CFD simulation parameters.

Parameter	Churning losses simulations	Squeezing losses simulations
Pressure-velocity coupling	SIMPLE	SIMPLE
Simulation type	Laminar	Turbulent (turbulence model RNG k–ε)
Energy equation	Not activated	Not activated
Mesh type	Sweep	Tetra
Free surface tracking method	VoF	VoF
Solver	Pressure based	Pressure based
Time	Transient	Transient
Spatial discretization		
– Gradient	Least-squares cell based	Least-squares cell based
– Pressure	Standard	Standard
– Momentum	Second-order upwind	Second-order upwind

CFD: computational fluid dynamics; RNG: re-normalization group; VoF: volume of fluid.

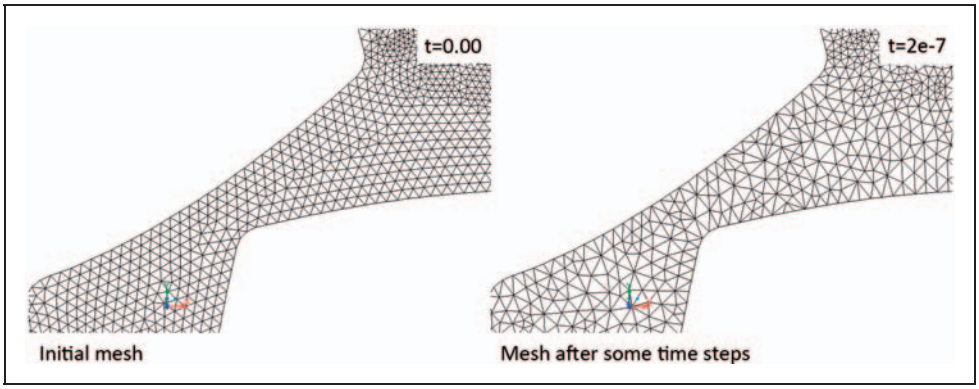

Figure 5. An example of the results obtained by the remeshing technique adopted. On the left, initial mesh before any boundary motion; on the right, after some time steps ($T = 2.0\,e{-}07$) the shape of the mesh is changed in order to find a new equilibrium state in which the deformation of the elements due to the boundary motion is equally distributed between all the elements (without the smoothing, the cells near the boundaries will immediately collapse because they will carry out the whole deformation).

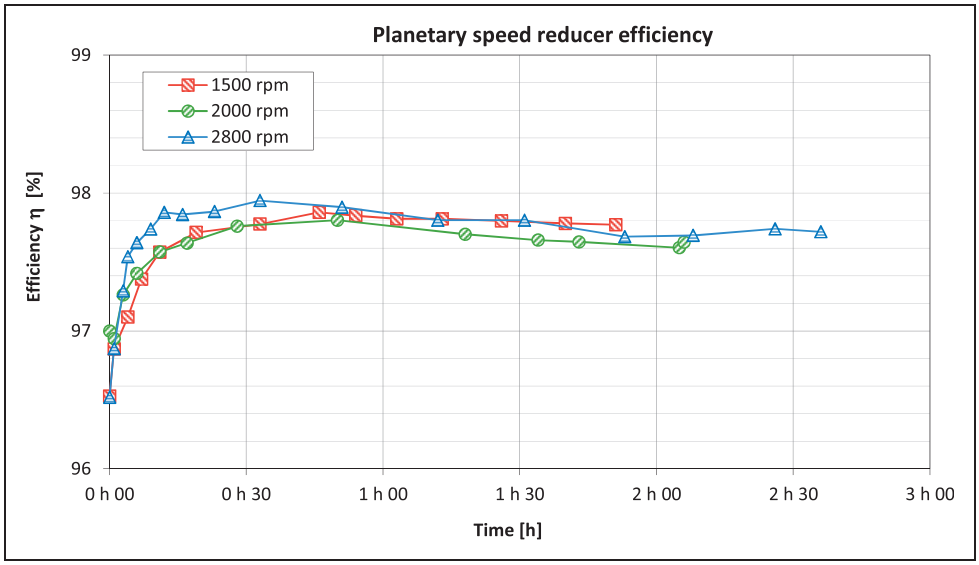

Figure 6. Variation of the measured efficiency of the planetary speed reducer over test time for three different rotational speeds of the input shaft (1500, 2000 and 2800 r/min).

In Figure 8, the bar diagram shows a comparison between measured and calculated power losses of the speed reducer split up in load-dependent and load-independent components. The predicted power losses were determined by means of the calculation methods proposed in references[13,14] integrated by CFD results.

In terms of absolute quantities, the value of the total power loss experimentally determined increases more than linearly with the increase in the input shaft rotational speed at the same applied braking torque. The calculated values of total power loss capture the same trend, although some acceptable differences of about 10% are present. While, in terms of percentage of power losses over the transmitted power, the three different test conditions lead to results that are in very close agreement with both the experimental and numerical results. The subdivision in load-dependent and load-independent power losses is also practically independent of the rotational speed and shows clearly the important role played by the load-independent power losses in this type of speed reducer since the contribution to the total power loss of no-load losses was only slightly lower than one of the load-dependent power losses. Comparing the measured and the calculated load-independent power losses, it can be noticed that the measured power losses are, for all the three test conditions, higher than the calculated ones. In any case there are only slight differences between calculated and measured values and these differences are of the same magnitude of the ones between the measured and the calculated load-dependent power losses.

Considering the calculated power losses, a subdivision of the total power loss in different contributions given by the different mechanical elements is possible

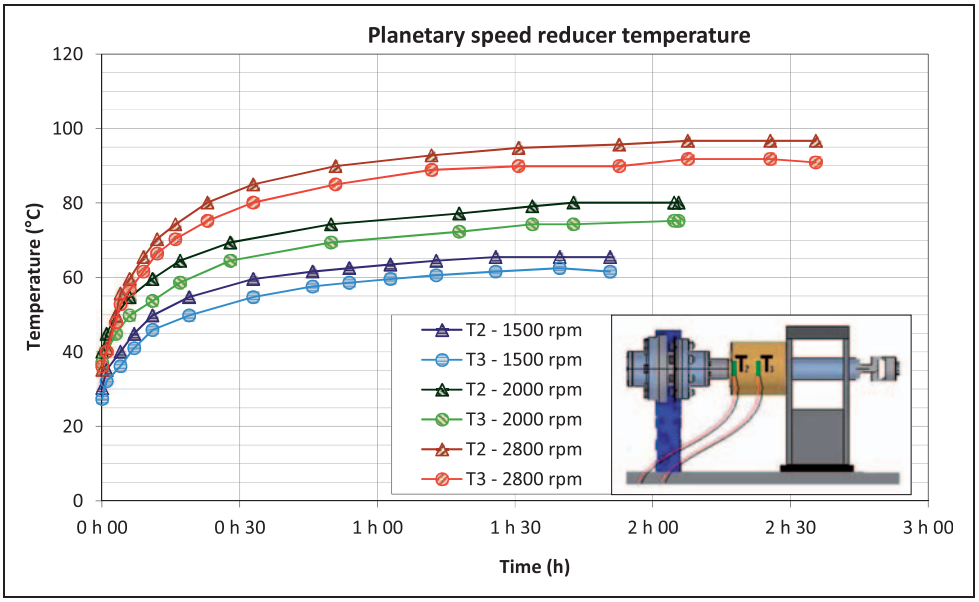

Figure 7. Variation of the measured temperatures of the planetary speed reducer case over test time for three different rotational speeds of the input shaft (1500, 2000 and 2800 r/min).

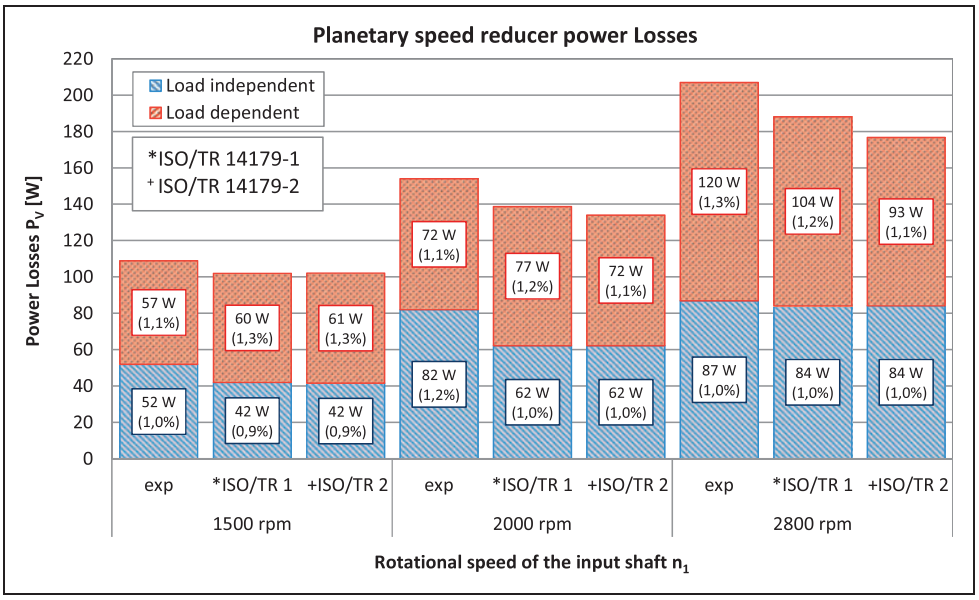

Figure 8. Measured and calculated steady-state power losses of the planetary speed reducer.

as shown in Figure 9. The gears gave the major contribution to the load-dependent, as well as to the load-independent power losses in all the three different operating conditions analyzed. The rolling bearings gave a contribution to the total power loss in the speed reducer that was significantly lower than one of the gears. This fact can be explained since the four roller bearings that are mounted on the input and output shafts are not loaded due the transmitted torque. In fact, in this particular planetary speed reducer configuration, in which three planets are present, the forces acting on the input and output shafts are internally balanced so that these ball bearings are loaded only by the weight of shafts, gears, planet carrier and the rotating body of the HBM T12 torque meter. The power losses generated by the contact seals gave an important contribution close to one of the bearings.

Concerning the gear power losses, in this type of speed reducer, the contribution of the load-independent gear power losses is significant as they are about 50% of the load-dependent gear

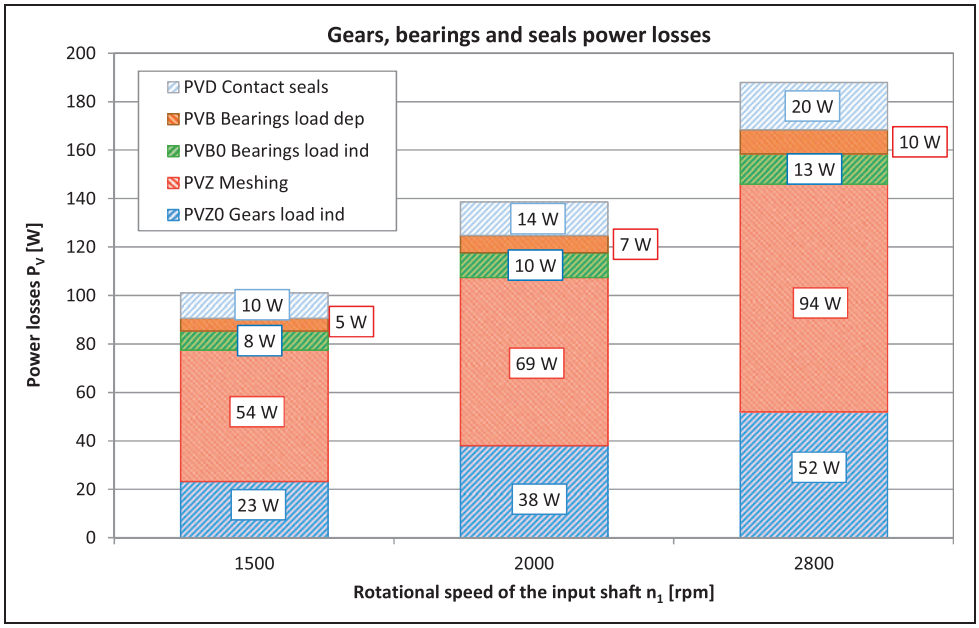

Figure 9. Calculated steady-state power losses in the planetary speed reducer coming from gears, bearings and seals.

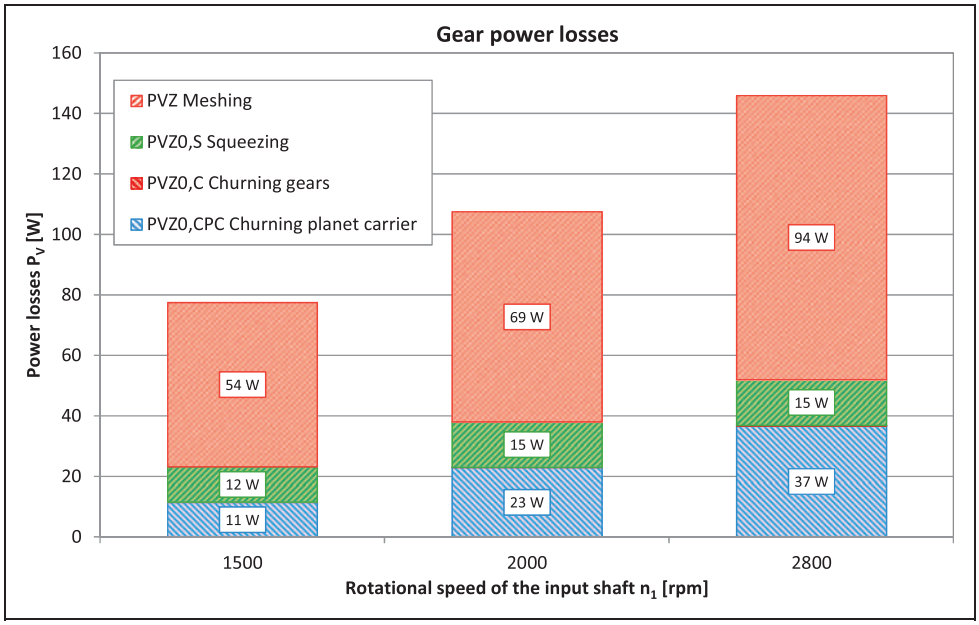

Figure 10. Calculated steady-state gear power losses in the planetary speed reducer split up in different contributions.

power losses. A significant contribution to the no-load power losses of gears was given by the squeezing power losses. The largest contribution to this kind of power losses was given by the churning losses due to the rotation of the planet carrier (see Figure 10), while the churning losses due to the rotations of gears about their axes were negligible. Considering that the power losses of the carrier is strictly dependent on lubricant properties and on speed reducer internal layout, the importance in defining possible solutions for power losses reduction of a CFD approach that is able to take into account the influence of these parameters is clear.

Conclusions

A testing campaign was performed in order to measure the global efficiency of an industrial planetary speed reducer in different operating conditions. The experimental results obtained were used as a basis to quantify the different contributions to the total power loss of the speed reducer coming from different sources, as well as to check the availability of reliable prediction model for each of them. Based on the results of such investigation, load-independent gear losses have proven to be quantitatively important, to have significant margins of improvement and to be lacking

of reliable prediction models. For this reason, taking into account the recent developments of CFD, the related hardware and software tools and the previous experiences of the authors for ordinary gears, CFD simulations have been proposed as a possible approach to investigate such kind of losses. The comparison of the theoretical predictions with the experimental tests performed on the same gearbox has been provided, also for the specific case of planetary gearboxes, a validation of the approach to the no-load losses based on CFD simulations, and, in general, a comprehensive validation of the whole approach.

Funding

This research received no specific grant from any funding agency in the public, commercial or not-for-profit sectors.

Conflict of interest

None declared.

Acknowledgments

The authors gratefully acknowledge the support given by Bonfiglioli Group to this research. They especially wish to thank Rodolfo Arigoni and Mauro Musolesi from the Tecnoingraggi division of the Bonfiglioli Group for their cooperation in the design of the experimental campaign.

References

1. Niemann G and Winter H. *Maschinenelemente. Band 2: Getriebe allgemein, Zahnradgetriebe - Grundlagen, Stirnradgetriebe*. Berlin, Germany: Springer-Verlag, 1983.
2. Dawson PH. Windage loss in larger high-speed gears. *Proc IMechE Part A: J Power and Energy* 1984; 198: 51–59.
3. Diab Y, Ville F and Velex P. Investigations on power losses in high speed gears. *Proc IMechE Part J: J Engineering Tribology* 2006; 220: 191–198.
4. De Gevigney JD, Ville F, Changenet C, et al. Tooth friction losses in internal gears: analytical formulation and applications to planetary gears. *Proc IMechE Part J: J Engineering Tribology* 2013; 227: 476–485.
5. Ohlendorf H. *Verlustleistung und Erwörmung vons Stirnrödern*. PhD Thesis, TU München, Germany, 1962.
6. Mauz W. *Hydraulische Verluste von Stirnradgetrieben bei Umfangsgeschwindigkeiten bis 60 m/s*. PhD Thesis, Universität Stuttgart, Germany, 1987.
7. Terekhov AS. Hydraulic losses in gearboxes with oil immersion. *Vestnic Mashinostroeniya* 1975; 55: 7–11.
8. Walter P and Langenbeck K. *Anwendungsgrenzen für die Tauchschmierung von Zahnradgetrieben, Plansch- und Quetschverluste bei Tauchschmierung*. Report, FVA Forschungsvorhaben Nr. 44/1, Frankfurt, 1982.
9. Walter P. *Untersuchungen zur Tauchschmierung von Stirnrädern bei Umfangsgeschwindigkeiten bis 60 m/s*. PhD Thesis, Universität Stuttgart, Germany, 1987.
10. Changenet C and Velex P. A model for the prediction of churning losses in geared transmissions - preliminary results. *ASME J Mech Des* 2007; 129: 128–133.
11. Gorla C, Concli F, Stahl K, et al. CFD simulations of splash losses of a gearbox. *Adv Tribol* 2012; 2012: 616923 (10 pages).
12. SKF. General catalog. Catalogue 6000/I EN, June 2008.
13. ISO/TR 14179-1:2001. Gears – thermal capacity – part 1: rating gear drives with thermal equilibrium at 95°C sump temperature.
14. ISO/TR 14179-2: 2001. Gears – thermal capacity – part 2: thermal load-carrying capacity.
15. Concli F and Gorla C. Computational and experimental analysis of the churning power losses in an industrial planetary speed reducer. In: *9th international conference on advances in fluid mechanics – advances in fluid mechanics IX,* Split, Croatia, 26–28 June 2012, vol. 74, pp.287–298. Southampton, UK: WIT.
16. Versteeg HK and Malalasekera W. *An introduction to computational fluid dynamics – the finite volume method*. London, UK: Longman Group, 1995.
17. Yakhot V, Orszag SA, Thangam S, et al. Development of turbulence models for shear flows by a double expansion technique. *Phys Fluids A* 1992; 4: 1510–1520.
18. Concli F and Gorla C. Analysis of the oil squeezing power losses of a spur gear pair by means of CFD simulations. In: *Proceedings of the ASME 11th biennial conference on engineering systems design and analysis*, Nantes, France, 2–4 July 2012, vol. 2, paper no. ESDA2012-82591, pp.177–184. New York, NY: ASME.